ELSEVIER

Journal of Nuclear Materials 318 (2003) 56–69

journal of nuclear materials

www.elsevier.com/locate/jnucmat

Summary of the results from post-irradiation examination of spent targets at the FZ-Juelich

J. Chen [a,*], G.S. Bauer [a], T. Broome [b], F. Carsughi [c], Y. Dai [d], S.A. Maloy [e], M. Roedig [a], W.F. Sommer [e], H. Ullmaier [a]

[a] *Projekt ESS, Forschungszentrum Jülich, D-52425 Jülich, Germany*
[b] *Rutherford–Appleton Laboratory, Chilton OX 11 0QX, UK*
[c] *DIBIAGA, University of Ancona, I-60131 Ancona and INFM Unitá di Ancona, Italy*
[d] *Spallation Source Division, Paul-Scherrer-Institut, CH-5232 Villigen, Switzerland*
[e] *APT/TPO, MS H809, Los Alamos National Laboratory, NM 87545, USA*

Abstract

The lifetime of structural components of spallation targets (beam window, liquid metal container, return hull) is determined by the irradiation-induced changes of the mechanical properties of their materials. An extensive test program was initiated using specimens obtained from spent target components from operating spallation facilities (Los Alamos Neutron Science Center, LANSCE and the Spallation Neutron Source at Rutherford–Appleton Laboratory, ISIS). The investigated materials include a nickel-based alloy (IN 718), an austenitic stainless steel (AISI 304L), a martensitic stainless steel (DIN 1.4926) and a refractory metal (tantalum). The materials experienced 800 MeV proton irradiation to maximum fluences of $>10^{25}$ p/m^2. The mechanical property changes were investigated by microhardness measurements, three-point bending tests and tensile tests at temperatures ranging from room temperature (RT) to 250 °C. Subsequent scanning electron microscopy was employed to investigate the fracture surfaces. Generally, irradiation hardening and a decrease in ductility with increasing proton fluence was observed. Nevertheless, all materials except IN 718 tested at RT, retained some ductility up to the maximum doses explored. The transmission electron microscopy investigation showed that a high density of 'black dots' and dislocation loops appeared in all materials. No effect of long-range radiation-induced segregation at grain boundaries was detected by energy dispersive X-ray investigation on AISI 304L and IN718 which failed by intergranular fracture.

1. Introduction

Because of their unique advantages in time-of-flight based neutron scattering measurements, the next generation of high intensity neutron sources will be pulsed spallation sources. In such accelerator-driven facilities, the neutrons are generated by a high energy (≈1 GeV) and intense current (>1 mA) proton beam which induces spallation of the nuclei in a heavy metal target. In both the planned European Spallation Source (ESS) [1] and the Spallation Neutron Source (SNS) [2] under construction in the United States, a liquid mercury target, combining high neutron production efficiency and heat removal capability, has been chosen, where typical operating temperatures range from 100 to 250 °C. Very high pulsed power densities will be deposited in the target structural materials, leading to severe thermal, mechanical and radiation loads in the beam window, mercury container, return hull, and associated components.

Concerning radiation damage, the most critical regions of the target structure will be the ones penetrated by the proton beam. Typical, the centre of the target window would accumulate a proton fluence of

* Corresponding author. Address: Institut fur Festkorperforshcung, Forschungszentrum Jülich, Jülich 52425, Germany. Tel.: +49-2461 612473; fax: +49-2461 614413.
E-mail address: j.chen@fz-juelich.de (J. Chen).

0022-3115/03/$ - see front matter
doi:10.1016/S0022-3115(03)00007-2

1.6×10^{26} p/m^2 within one year of full power operation of ESS. In steels this leads to a displacement dose of about 60 displacements per atom, dpa, and a helium concentration of almost 1 at.%. Depending on the location in the target region considerable fluences of fast neutrons will add to these numbers. Based on ample experience in the development of fission and fusion materials it was expected that hardening and low temperature embrittlement should be the main changes in the mechanical properties for the anticipated temperature range. However, it is not possible to transfer fission and fusion data quantitatively to the spallation case characterized by extremely high helium/hydrogen to dpa ratios and primary knock-on energies. Irradiations and tests under conditions typical for spallation targets are thus required.

The fastest way to develop a database for spallation materials appeared to be the investigation of specimens obtained from spent targets of already operating medium-power sources. Beginning in 1996, spent target components from LANSCE (Los Alamos Neutron Science Center) and ISIS (Spallation Neutron Source at Rutherford–Appleton Laboratory) were collected. The available materials included four different alloys: an austenitic stainless steel (AISI 304L), a nickel-based alloy (IN 718), a martensitic stainless steel (DIN 1.4926) and a refractory metal (tantalum). The specimen preparation and the measurements were mainly performed in the hot cells of the Forschungszentrum Jülich. Several mechanical tests, including hardness, bending and tensile tests were conducted. The fracture surfaces were observed by scanning electron microscopy (SEM) after bending and tensile tests. The changes of the microstructures after irradiation were investigated by TEM. This paper presents a brief summary of the investigation programme.

2. Materials and irradiation

The investigated spent targets and components are a LANSCE Water-Degrader, a LANSCE Beam-Window, a Paul-Scherrer-Institut, PSI-Window irradiated in LANSCE and an ISIS target. The details of the materials, dimensions and the operation conditions can be found in Refs. [3–7]. Only a brief description is given here. The Water-Degrader consisted of two concentric spherical shells made of IN 718 (outer shell) and AISI 304L (inner shell), respectively. It was placed between the proton beam entry window and the isotope production targets in the beam stop area of LANSCE and was used as a neutrino source. In the operation period from October 1988 to September 1993, the Water-Degrader was irradiated with 760 MeV protons to a total charge of 5.3 A h at a maximum temperature of 250 °C. The LANSCE Beam-Window made of IN 718 is a hemispherical double-shell with cooling water flowing between the two shells and was used to separate the vacuum of the beam line and the target area. It was installed in the beam line of the LANSCE accelerator in April 1995. From that time until it was removed from service in 1997, it was exposed to a total charge of ≈3.4 A h at around 400 °C. The water-cooled double-shell PSI-Window was manufactured in the Paul Scherrer Institut, Switzerland and irradiated in LANSCE from June, 1989 to October, 1990 with 800 MeV protons to a total charge of 2.8 A h at $\leqslant 230$ °C. The ISIS target consisted of a target container with a window made of a AISI 304L stainless steel and 23 water-cooled Ta plates which served as spallation material. During service in the period 1988–1994, the target was irradiated with a short-pulsed 800 MeV proton beam at temperatures lower than 200 °C. The total accumulated charge on the target was 1.7 A h. Chemical compositions of the different materials are given in Table 1.

To specify the irradiation conditions, the profiles of the proton beam impinging on the spent target components were measured by γ-scans in the hot cells of FZ-Juelich. It was found that the positron decay of Na^{22}, Ti^{44} and Co^{57} was mainly initiated by the proton beam in Ni- and Fe-based alloys. Therefore the integrated positron decay distributions were used to obtain the proton beam profile, showing that the intensity distributions of the proton beam at all components had a

Table 1
Chemical composition of investigated materials (wt%)

Alloy	Fe	Cr	Ni	Mo	Mn	Nb	Si	C	N	O	Ta
AISI 304L[a]	Bal.	18–20	8–12	–	<2.0	–	<1.0	<0.08	–	–	–
IN 718[a]	18	18	Bal.	3	0.46	5	–	–	–	–	–
DIN 1.4926	Bal.	10.5	0.64	0.9	–	0.01	0.36	0.2	–	–	–
Ta	–	–	–	2[b]	–	10[b]	–	20[b]	6[b]	8[b]	>99.99

[a] Nominal.
[b] wt-ppm.

Table 2
Irradiation conditions

	LANSCE Water-Degrader		LANSCE Beam window	PSI-Window	ISIS target
	IN 718	AISI 304L	IN718	DIN 1.4926	Pure Ta
Protons (A h)	5.29	5.29	3.41	2.83	1.74
σ_x/σ_y (mm)	–	22.6/28.8	–	16.3/23.6	17.0/20.7
Peak fluence (p/m^2)	2.9×10^{25}	2.9×10^{25}	6.4×10^{25}	2.6×10^{25}	1.7×10^{25}
Max. irrad. temp. (°C)[a]	250	250	400	250	200
Max. dpa	8.5	8.5	20	6.8	11
Max. He (appm)	1510	1680	3330	1510	580
Max. H (appm)[b]	5890	5270	13 000	4720	–

[a] The Max. irrad. temp. refers to the maximum temperature which the component has experienced in the beam center and operating the spallation neutron source at maximum power.

[b] The values represent the hydrogen produced in materials. But there are energetic losses and diffusional losses depending on geometry of the parts, the solubility and diffusivity of hydrogen, and the microstructural sinks in the materials.

two-dimensional Gaussian shape with variances σ_x and σ_y, respectively (see Table 2). From the parameters of the distributions and the total charges, peak proton fluences of 2.9×10^{25} p/m^2 for the Water-Degrader, 6.4×10^{25} p/m^2 for LANSCE-Window, 2.6×10^{25} p/m^2 for PSI-Window and 1.7×10^{25} p/m^2 for ISIS target were obtained for the beam centres. Taking a displacement damage cross-section of 2900 b for 304L and IN 718 [8], 2600 b for DIN 1.4926 [9] and 6650 b for Ta [10], the maximum displacement doses are 8.5, 20, 6.6 and 11 dpa for 304L, IN 718, DIN 1.4926 and pure Ta, respectively. To determine the He- and H-concentrations in the materials, the production cross-sections of $\sigma_{He} = 0.58$ b and $\sigma_H = 1.8$ b for 304L and DIN 1.4926 [11], $\sigma_{He} = 0.52$ b and $\sigma_H = 2.0$ b for IN 718 [11] and $\sigma_{He} = 0.34$ b for Ta [10] were used, and the resulting maximum He- and H-concentrations are found to be 1680 and 5270 appm for 304L, 3330 and 13 000 appm for IN 718 and 1510 and 4720 appm for DIN 1.4926, respectively. Because of the unknown cross-section of H-production in Ta, only the He-concentration is calculated to be 580 appm. A summary of the irradiation conditions is given in Table 2. It should be noticed that the contribution of the fast neutrons to dpa and transmutation products is not included. At the position of the Water-Degrader, the LANSCE- and the PSI-Window, the flux of neutrons was very low and their contributions were estimated to be less than a few percent of the proton-induced values in the beam centre, while it is somewhat higher in the case of the ISIS target.

3. Microhardness

The high gradient of the irradiation dose across the components suggested that microhardness measurements would be very useful to follow the changes in mechanical properties induced by the irradiation, due to the very low volume of material used in each measurements. The data obtained by hardness tests are not directly used for any engineering purpose, but information on the trend of changes of mechanical properties offers important indications for material problems. The hardness tests were not performed on the surface of the components for the following reasons: (1) the surface of the component might not be flat and hence the measurements had to deal with this complication, (2) the bulk material was certainly not affected by any surface problems due to the presence of cooling media or direct proton beam exposure. By cutting a sample from the component, a perfect flat surface for the measurements was available.

Moreover, in order to deal with a high dose gradient, microhardness tests were performed with a load of 2 N (HV 0.2) and the results on each position have been averaged over several indentations along the thickness. The change of the hardness as a function of the position on the component aided determination of the average proton beam dimension. Actually, an estimated proton beam dimension of 21 ± 4 mm from microhardness-position data for the Water-Degrader is in good agreement with the γ-scans measurement given in Table 2.

In Fig. 1, the hardness data of the four different materials are shown and compared. First of all, attention is drawn to the IN 718 material, which is the only one that, after a hardening regime up to about 1–2 dpa, shows a softening at higher doses. This is due to the dissolution of the γ' and γ'' precipitates which are responsible for the high strength of the unirradiated material at high temperature [12,13]. The ordered phases fcc LI_2 and bct DO_{22} survive only less than a few dpa of high energy proton irradiation and this is reflected in the softening of the material. The hardness level of IN 718 after about 8 dpa is still comparable with that one of DIN 1.4926 (about 400 HV 0.2), but the trend of the two materials is rather different. All the other three materials,

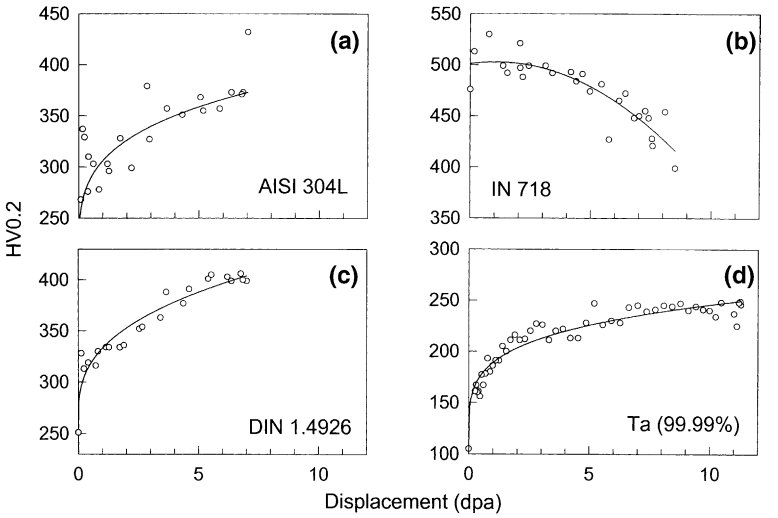

Fig. 1. Dependence of Vickers microhardness HV0.2 at RT on displacement dose for (a) AISI 304L, (b) IN 718, (c) DIN 1.4926 and (d) Ta.

i.e. AISI 304L, DIN 1.4926 and Ta, show hardening after irradiation. Both steels reach the level of 400 HV 0.2 at about 7 dpa, while the pure Ta reaches only about 250 HV 0.2 at 11 dpa.

4. Three-point bending

Due to the difficulties in handling miniaturized specimens inside the hot cells, the investigations on the irradiated materials were started with three-point bending samples of $15 \times 2 \times 3$ mm^3 in size. This technique was preferred to the more standard four-point bending in order to keep the sample as small as possible because the high gradient of the irradiation dose prevents a constant level of irradiation inside a larger specimen. By this method it was possible to attribute the mechanical properties to a defined set of irradiation parameters. The tests were performed with a 5 KN load cell and with a crosshead speed of 0.2 mm/min. The experimental setup allowed a maximum deflection of about 2 mm. In order to take into account differences due the sample dimension on the experimental curve, calibrations with unirradiated samples of different dimension were performed [3]. The data obtained by different samples scale with a parabolic function of bh^2 (b is

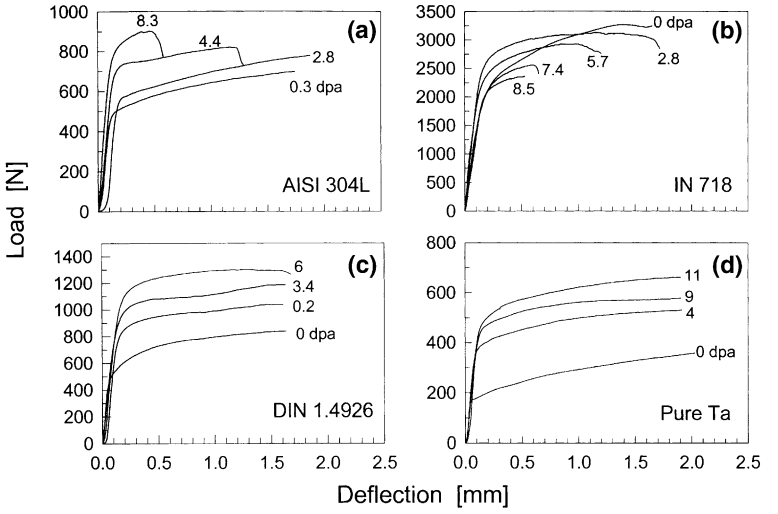

Fig. 2. Three-point bending curves of (a) AISI 304L, (b) IN 718, (c) DIN 1.4926 and (d) pure Ta in dependence of irradiation.

the width of the bend bar and h is its height) and this calibration curve was used to normalize the data obtained from the irradiated samples. One of the major problems in these investigations was related to the reference unirradiated material. Components were operated for years in spallation environments, and no archive material was left for comparison. Therefore, material having similar composition and heat treatment was used as reference material.

The results of the three-point bending test gave qualitatively similar indications as observed with the microhardness tests, and the whole set of curves is shown in Fig. 2. The IN 718 samples did show a trend for softening (the first sample tested had reached an irradiation dose of 2.1 dpa) as already pointed out by microhardness tests; moreover in this case a reduction of ductility was also observed. All the other materials, i.e. AISI 304L, DIN 1.4926 and pure Ta, did show a hardening with a reduction of ductility. Among the steels, the austenitic one, AISI 304L, showed a much larger reduction in ductility already visible in the hot cell window: the sample irradiated up to about 8.3 dpa broke after 0.5 mm of deflection. On the other hand, the martensitic one, DIN 1.4926, irradiated up to about 6.8 dpa did not break under the same experimental conditions. The results for pure Ta were surprising; a highly brittle material was expected, but the results show instead an irradiation hardening but no reduction of ductility under the given experimental condition. Even the sample irradiated up to 10 dpa did not break during the three-point bending test but showed an extreme ductile behaviour and could be bent end to end without failure (Fig. 3). The Ni base superalloy, IN 718, showed a trend for softening, but the values of the failure loads were still much higher than for the other materials, although the reduction in ductility was rather strong at 8.5 dpa.

5. Tensile

Best quantitative information of the strength and ductility of the materials is achieved with tensile tests which were also performed in the hot cells. Considering the high spatial gradient of the proton beam, miniature-type flat dog-bone tensile samples were chosen to avoid large dose variations along their length. The tensile specimens were machined from spent components to

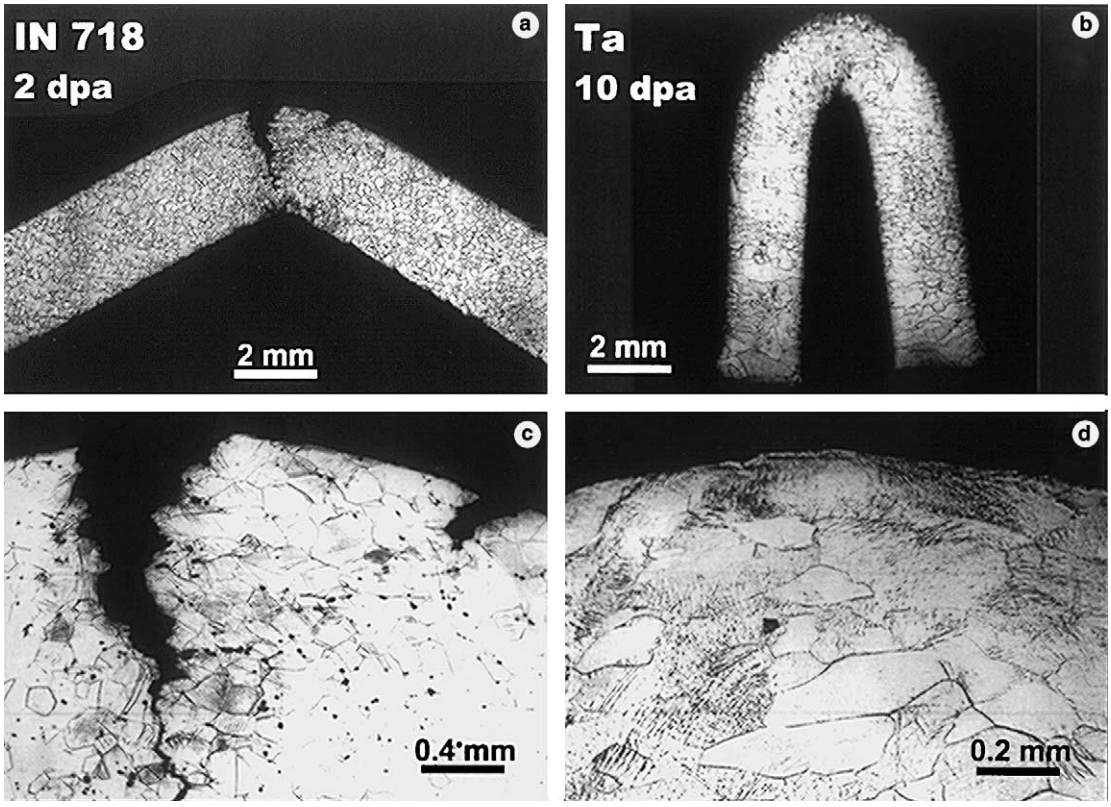

Fig. 3. Optical micrographs of a IN 718 sample irradiated to 2 dpa after bending test ((a), (c)) and a Ta sample irradiated to 10 dpa after bending end to end ((b), (d)).

about 0.5 mm thickness, 5 mm length and 1.2 mm width in the gauge region. The tensile tests were performed at room temperature (RT, 25 °C), 164 °C and 250 °C in air, respectively, using a 2 kN MTS tensile machine equipped with a video-extensometer in order to measure the elongation directly in the gauge area. The strain rate was about 10^{-3} s^{-1}.

Typical stress–strain curves of AISI 304L before and after irradiation are shown in Fig. 4(a), (b) and (c), corresponding to the test temperatures of 25, 164 and 250 °C, respectively. The tensile curves showed irradiation hardening and concomitant loss of ductility at all three test temperatures. At test temperature of 25 °C, the yield stress increased rapidly with displacement dose at the beginning and then followed a relatively slow increase at higher doses with a tendency to saturation at around 800 MPa at 5–6 dpa. This value was reduced to around 700 MPa at elevated temperatures. On the other hand, the retained ductility changed irregularly with test temperature, i.e. from total elongation of 8% at 25 °C, to 25% at 164 °C and to 12% at 250 °C. One should also notice that irradiation induced a serious loss in work hardening ability. Because of the almost zero work hardening rate for irradiation to high dpa and test temperatures of 164 and 250 °C (cf. Fig. 4(b) and (c)), it was difficult to determine the uniform elongation. Moreover the direct of comparison of uniform elongation from different curves might exaggerate the difference of the ductility. For comparison, two curves of AISI 316L irradiated by 800 MeV protons to 9 dpa at 164 °C [14] and irradiated by fast neutrons to 10 dpa at 250 °C [15] are included in Fig. 4(b) and (c), respectively. The comparison shows a higher strength for AISI 316L compared to AISI 304L but the former shows a lower ductility after irradiation.

Representative stress–strain curves for IN 718 after irradiation are shown in Fig. 5. Fig. 5(a) and (c) are results from the LANSCE-Window tested at 25 and 250 °C, respectively. Fig. 5(b) is a previous result gained earlier in the irradiation programs for the Accelerator Production of Tritium (APT) project [14]. Since no unirradiated material from the same heat as used for the LANSCE-Window was available, samples cut from the rim part of the window were used as a reference. They were outside the proton beam area, and had very little irradiation exposure. According to the curves in Fig. 5(a), IN 718 shows an irradiation hardening at the early stages of the irradiation, followed by irradiation softening beyond about 2 dpa. A more remarkable effect is the drastic reduction in elongation with increasing dose. In particular, the 20 dpa sample failed in the elastic region. At higher test temperatures, the curves show that the strength is slightly decreased but the ductility remain higher than in the RT tests.

The tensile properties of DIN 1.4926 in the tempered condition before and after irradiation are illustrated in Fig. 6(a) and (c) for test temperatures of 25 and 250 °C, respectively. A previous result on modified 9Cr1Mo steel [14], a quite similar material, irradiated and tested at 164 °C is included in Fig. 6(b). It can be seen that the strength is increased with the irradiation dose. The material loses its work hardening capability and begins necking after small strain <1% at a very low irradiation dose. However, the total elongation remains almost constant after a first drastic drop at the beginning of the irradiation. The yield strength was slightly reduced with increasing test temperature and the stress drops less steeply. Nevertheless, test temperature did not influence the total elongation up to 250 °C.

Fig. 7 presents the typical tensile curves of pure Ta before and after irradiation in a spallation environment. Irradiation causes significant strengthening and some reduction of elongation. Similar to DIN 1.4926, the drop in elongation occurred at dose below 0.6 dpa but up to the maximum available dose of 11 dpa the retained elongation has a much higher value (strain-to-necking of

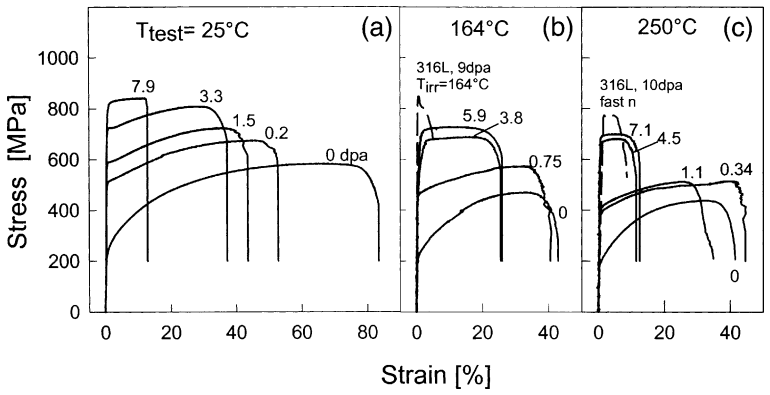

Fig. 4. Stress–strain curves of AISI 304L specimens, (a) tensile tested at 25 °C, (b) tensile tested at 164 °C, (c) tensile tested at 250 °C. Strain rate: 10^{-3} s^{-1}. For comparison two 316L curves are included in (b) and (c), respectively.

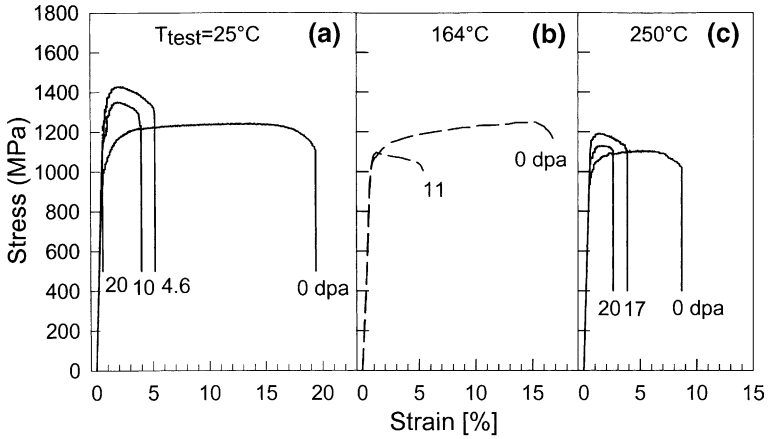

Fig. 5. Stress–strain curves of IN 718 specimens from the LANSCE-Window, (a) tensile tested at 25 °C and (c) tensile tested at 250 °C. Strain rate is 10^{-3} s^{-1}. The dashed lines in (b) indicated curves from the APT irradiation program [12].

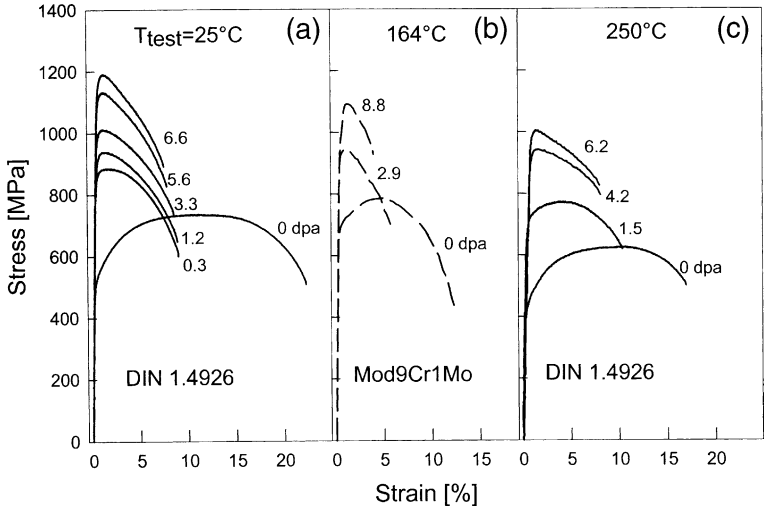

Fig. 6. Stress–strain curves of DIN 1.4926 specimens from the PSI-Window, (a) tensile tested at 25 °C and (c) tensile tested at 250 °C. Strain rate is 10^{-3} s^{-1}. The dashed lines in (b) indicated curves of Mod9Cr1Mo from the APT irradiation program [12].

8–10%) in comparison to DIN 1.4926 which has only 1–2% of uniform elongation at a dose of 7 dpa. At RT the unirradiated specimens show a slight work hardening which is reduced to almost zero in the specimen with 11 dpa. Such loss of work hardening is even more serious at 250 °C. The curves show already work softening at a dose of 0.6 dpa.

From the tensile curves described above, the yield strength and strain-to-necking can be obtained and are summarized in Fig. 8 for all materials investigated in this study. For lifetime considerations the proton fluence is a more meaningful parameter than the dpa number because the displacement cross-section of Ta is about 2.5 times higher than for steels. Therefore the yield strength and strain-to-necking are plotted as a function of proton fluence. With increasing fluence the yield strengths are increased except for IN 718 which shows a slight softening at higher doses. The strength of 304L, DIN 1.4926 and pure Ta after irradiation to proton fluences of 3×10^{25} p/m^2 were 4, 2.5 and 3 times higher, respectively, than in the initial state. The strain-to-necking of 304L decreased smoothly down to about 6% at the highest fluence. The strain-to-necking of DIN 1.4926 and pure Ta decreased rapidly at fluences below 3×10^{24} p/m^2 and then remained almost constant. The remaining strain-to-necking was around 2% for DIN 1.4926 but 10% for pure Ta. For IN 718 the strain-to-necking became zero at 25 °C and 2% at 250 °C at a fluence of 6×10^{25} (corresponding to 5 months full power operation of ESS).

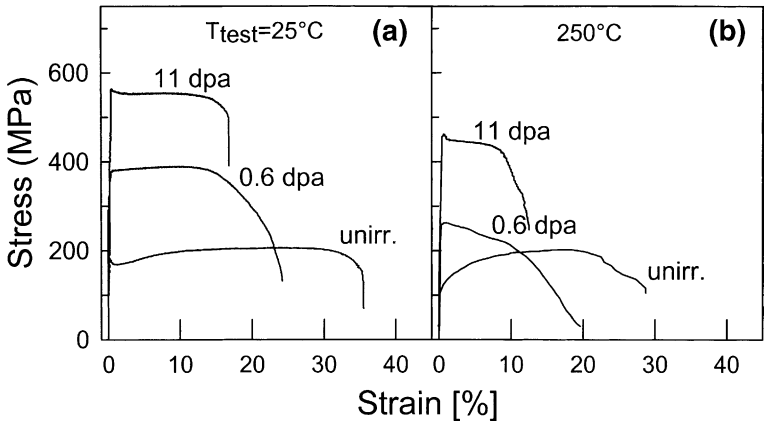

Fig. 7. Stress–strain curves of Ta specimens, (a) tensile tested at 25 °C and (b) tensile tested at 250 °C with a strain rate of 10^{-3} s^{-1}.

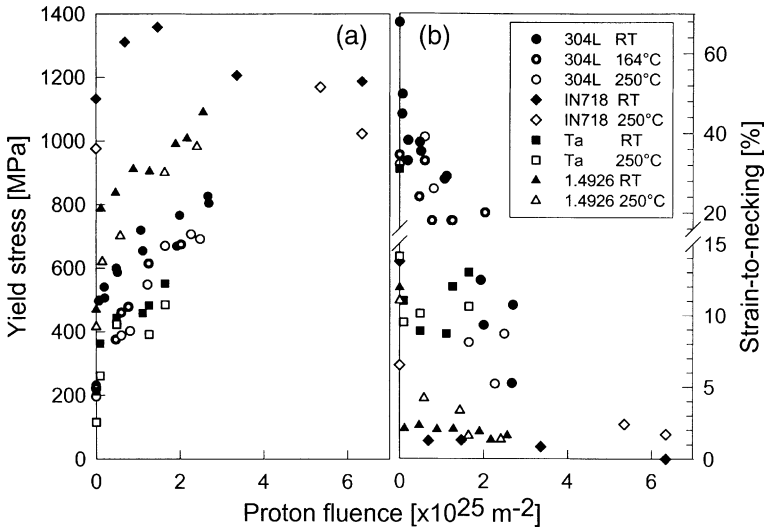

Fig. 8. (a) Yield strength and (b) strain-to-necking as a function of the proton fluence.

6. Scanning electron microscopy

Subsequent SEM investigations were performed after bending and tensile tests, to identify the fracture mode and the reduction in area. The SEM employed in the present studies is JEOL (JSM-6100) which quantify has been updated with a digital image processing system.

At a test temperature of 25 °C, the fracture mode of 304L changes gradually from pure ductile at 0 dpa to partial cleavage at 3.3 dpa and then to partial intergranular brittle mode at 8 dpa. It was found that the intergranular fracture covers a portion of about 60% on the fracture surface at 8 dpa [4]. When increasing the test temperature to 164 and 250 °C, the fracture surfaces of high dose samples became rough and dimpled, indicating ductile transgranular failure at elevated temperature. An example of the temperature dependence of fracture morphologies on 304L is shown in Fig. 9.

The fracture surfaces of the IN 718 specimen from the Water-Degrader tested in bending to failure at 25 °C show transgranular ductile fracture up to 6.8 dpa, a mixed mode at 7 dpa and fully intergranular at 8.5 dpa [3]. However, the fracture surfaces of the specimens from the LANSCE-Window show a transition from ductile to brittle only at 10 dpa and fully intergranular fracture behaviour at 20 dpa when samples are tested at 25 °C. The main difference between the Water-Degrader and the LANSCE-Window was the irradiation temperature, which was 250 °C for the former and 400 °C for the latter. If the test temperature is increased to 250 °C, the

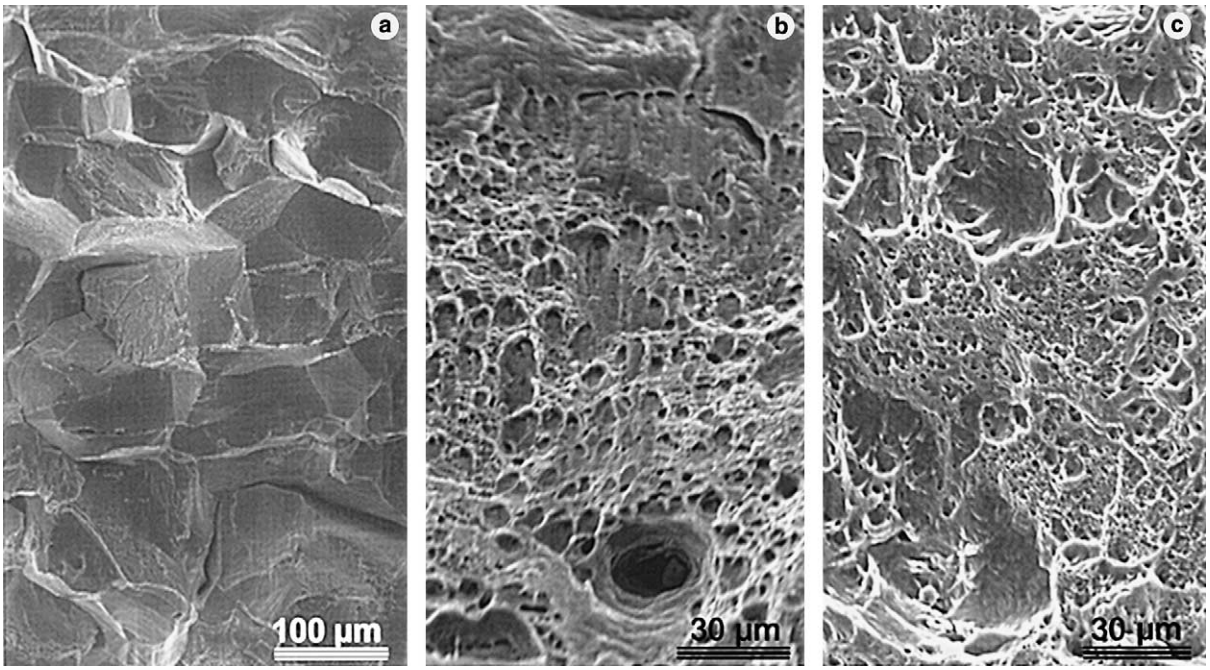

Fig. 9. Scanning electron micrographs showing the test temperature dependence of fracture surfaces of AISI 304L tensile specimens tested at (a) 25 °C with 7.9 dpa, (b) at 164 °C with 6 dpa and (c) at 250 °C with 7 dpa.

transgranular mode covers about 80% of the fracture surface of the 20 dpa sample. This phenomenon is illustrated in Fig. 10. It seems that the elevated operating temperature retarded the loss of ductility in IN 718.

SEM observation of DIN 1.4926 and pure Ta did not show any brittle fracture. The fracture mode of the DIN 1.4926 specimens was transgranular ductile before and after irradiation up to a displacement dose of 6.6 dpa at both test temperatures of 25 and 250 °C. The SEM observations show that chisels or pointed tips are formed during failure of the pure Ta reference specimen with almost 100% reduction in area at temperature of 25 and 250 °C, indicating that pure Ta is an excellent ductile material. This ductility was kept up to a dose of 11 dpa. This is demonstrated by a rough dimpled fracture surface observed in SEM investigations. The reduction in area of the irradiated samples with 10 dpa is retained to 56% and 61% at 25 and 250 °C, respectively.

Fig. 11 shows the reduction in area (RA) as a function of displacement dose for the different materials of this study. The general trend is a decrease in the RA with increasing displacement dose and in reverse with test temperatures. It should be emphasized that the RA of DIN 1.4926 was more than 50% at a dose of ~7 dpa whereas the uniform elongation was less than 2%. This indicates that the loss in work hardening as a result of irradiation causes local plastic deformations and as a consequence a reduced uniform elongation. It is not clear how to accommodate such kind of loss of ductility in the ESS target design.

7. Transmission electron microscopy

It is well accepted that mechanical property changes in irradiated materials are the direct result of the evolution of a damage microstructure. Therefore, in order to get a better understanding of the influence of irradiation effects on mechanical properties, transmission electron microscopy (TEM) was employed to investigate the microstructure changes during proton beam irradiation. The TEM specimens of 2.3 mm in diameter and 0.1 mm in thickness were prepared from the spent target components. Afterwards, the specimens were polished electrochemically in a Tenupol apparatus with a solution of 5 vol.% perchloric acid and 95 vol.% ethanol at a temperature of −20 °C and a current of 140 mA for 304L, IN 718 and DIN 1.4926. Ta specimens were polished with a solution of HF (42 ml), H_2SO_4 (125 ml), 2-butoxyethanol (139 ml) and methanol (700 ml) at −45 °C and a current of 100 mA. TEM examinations were conducted with a Philips TEM430 equipped with an energy dispersive X-ray (EDX) analysis system, operating at a voltage of 300 kV. The main image

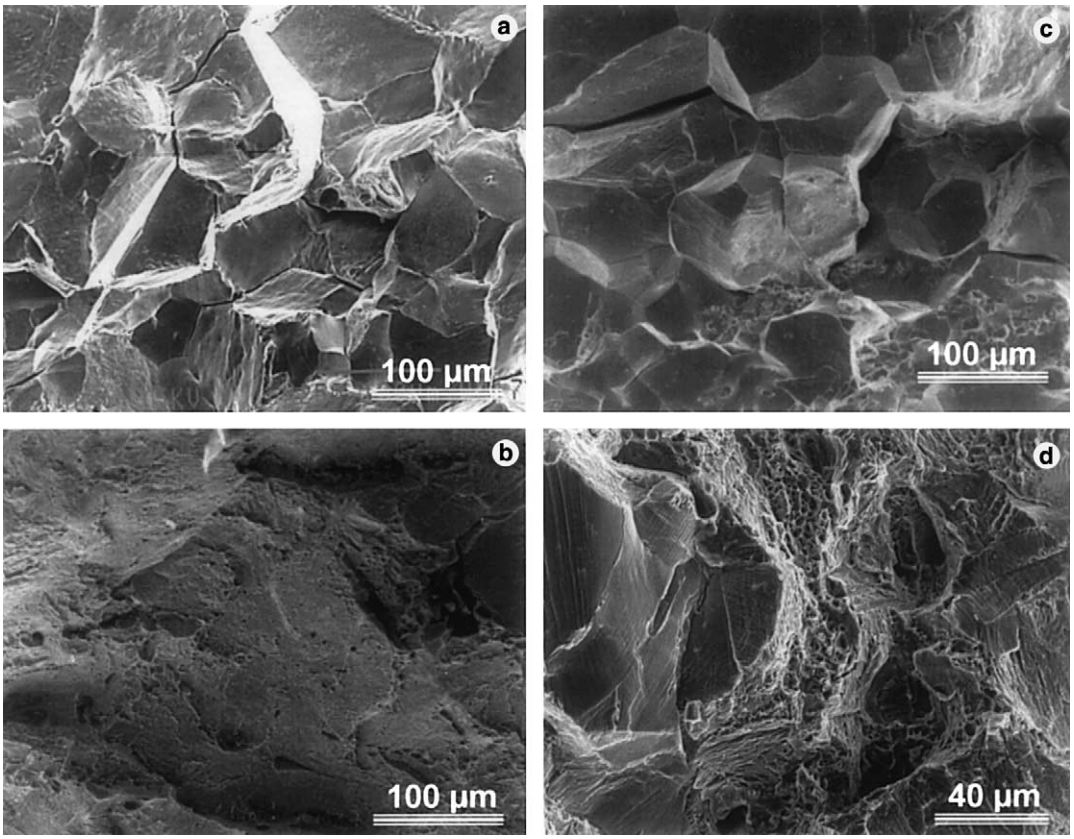

Fig. 10. Scanning electron micrographs showing the fracture morphology of IN 718 specimen (a) from the Water-Degrader with 8.5 dpa bending tested at 25 °C, (b) IN 718 specimens from LANSCE-Window with 10 dpa tensile tested at 25 °C, (c) with 20 dpa tested at 25 °C and (d) tested at 250 °C.

techniques were two-beam condition and weak beam dark field (WBDF) for loops and small clusters, phase contrast for bubbles and nano-size probe EDX spectroscopy for solute segregation.

Examples of typical microstructures in materials observed by TEM after 800 MeV proton irradiation in the low temperature regime are shown in Fig. 12. The detailed evolution of the microstructure with displacement dose can be found in Ref. [16] for 304L, [12] for IN 718 and [6] for DIN 1.4926. Here only a brief comparison of the four different materials is given. In 304L, the dominant microstructural feature is a high density of small 'black dot' defect clusters and faulted Frank dislocation loops. The densities of small clusters and loops were saturated at a dose of around 1 dpa. The cluster size remains constant at an average of 2 nm, but the loops continue to grow by net absorption of self-interstitials up to 23 nm at a dose of 8.5 dpa (cf. Fig. 12(a)). A remarkable change in IN 718 irradiated to 8.5 dpa was the disappearance of γ' and γ'' phases. The γ' and γ'' superlattice diffraction spots, clearly evident for unirradiated samples, were absent after irradiation. As in the case of 304L, a dense population of Frank-loops on $\{1\,1\,1\}$ habit planes and an average diameter of 15 nm were formed (Fig. 12(b)). On the contrary, the evolution of small clusters and loops is much slower in the bcc materials DIN 1.4926 and pure Ta than in the fcc materials 304L and IN 718. The density of defects in DIN 1.4926 is one order of magnitude lower than in 304L. The sizes of the defects were 5 and 3 nm in DIN 1.4926 and pure Ta, respectively, which is 5 times smaller than in 304L and IN718 (Fig. 12(c) and (d)). No bubbles were observed in all investigated of as-irradiated materials (resolution limit 1 nm).

Fracture surface observation has shown that the tensile specimens of 304L and IN718 failed by partial intergranular brittle fracture at 8.5 dpa. One possible reason for such weak bonds between the grains could be radiation-induced segregation (RIS) at the grain boundaries and solute enrichment or depletion at grain boundaries. The effect of RIS at GBs was investigated by dispersive energy microanalysis (EDX), using a probe diameter of 10 nm. Examples of microchemical profiles across the grain boundaries are shown in Fig. 13. The

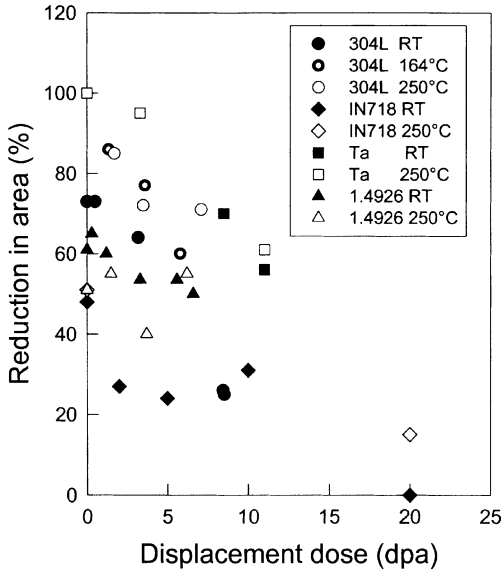

Fig. 11. Comparison of the reduction in area of AISI 304L, IN 718, DIN 1.4926 and high purity tantalum as a function of the displacement dose.

results show no long-range RIS within the resolution of 10 nm.

Auger electron spectroscopy (AES) of fracture surfaces samples much smaller depths. Measurements on IN 718 specimens [17] show much stronger enrichment of Ni and depletion of Fe and Cr near (<10 nm) grain boundaries in irradiated (8 dpa) specimens than observed in unirradiated material.

8. Discussion and summary

With respect to the importance of radiation damage effects for the lifetime of structural target components, information on the behaviour of their candidate materials in a spallation environment is urgently needed. Post-irradiation investigations of spent components from operating sources were considered to be the fastest way to obtain the initial data. Our results which are summarized in this report confirm this expectation. The most important general result is the finding that the 'hard' spectra of the bombarding protons and neutrons, respectively, and the accompanying high production rates of foreign elements do not cause qualitatively new radiation damage effects. This statement does not exclude an influence of those factors on quantitative aspects of irradiation-induced changes in the mechanical properties, especially at high doses.

As expected from ample experience in fission and fusion materials research, all investigated materials show strong irradiation-induced hardening and severe embrittlement. However, in most cases they maintain ductility and toughness values which should enable a

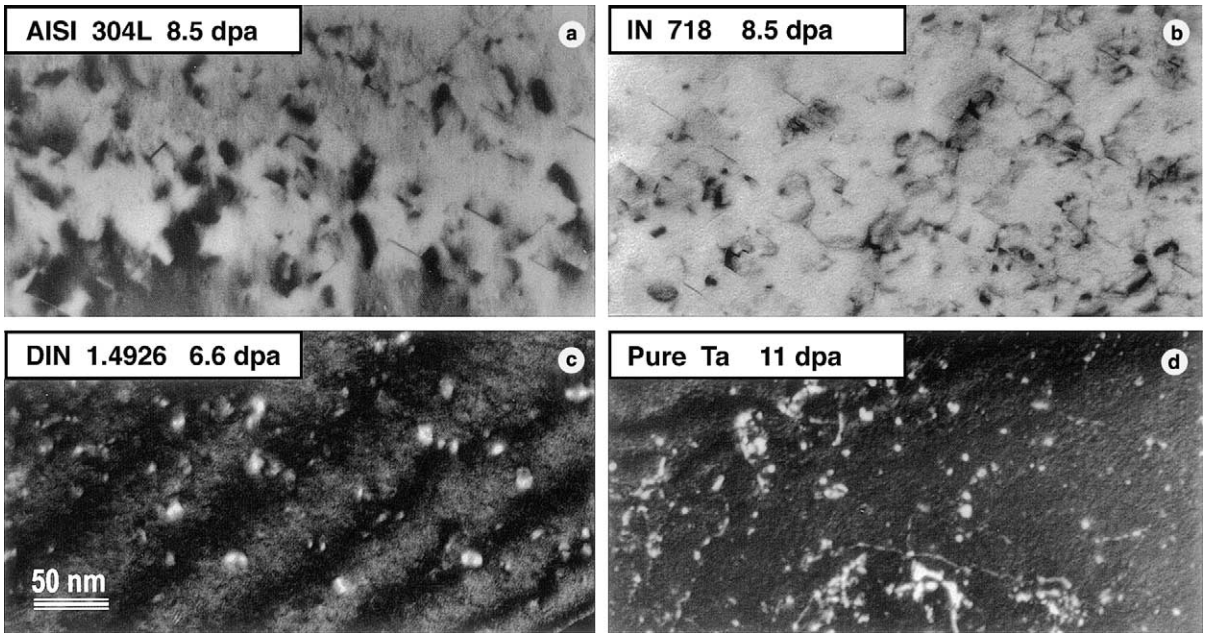

Fig. 12. TEM graphs showing four examples of the microstructural in samples. (a) AISI 304L with 8.5 dpa. (b) IN 718 from Water-Degrader with 8.5 dpa. (c) DIN 1.4926 with 6.6 dpa. (d) Pure Ta with 11 dpa. (a) and (b) are bright field images with $\mathbf{z} = 011$, $\mathbf{g} = 002$, (c) and (d) are weak beam dark field images $(\mathbf{g}, 4\mathbf{g})$ with $\mathbf{z} = 001$, $\mathbf{g} = 110$.

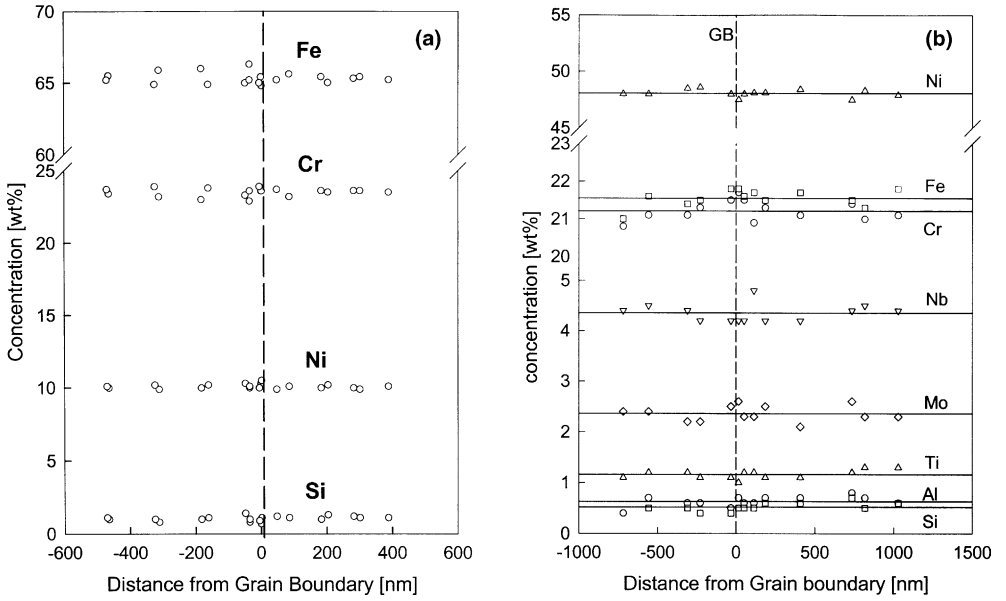

Fig. 13. Composition concentration profiles at the grain boundaries, (a) in AISI 304L with 8.5 dpa and (b) in IN 718 from Water-Degrader with 8.5 dpa.

design which ensures a safe and reliable function for the respective components. In somewhat more detail, the results can be summarized as follows:

(1) Microhardness, three-point bending and tensile tests on samples of AISI 304L, DIN 1.4926 and pure Ta showed irradiation hardening. In IN 718, small irradiation hardening occurred only up to 1–2 dpa and was followed by irradiation softening.
(2) All materials showed loss of ductility after irradiation. However, some ductility was retained, except for IN 718 tested at 25 °C. In particular, pure Ta showed an unexpectedly high ductility after irradiation.
(3) The fracture mode changed from typical ductile to partial and total intergranular failure for AISI 304L and IN 718, respectively. The transition dose increased with increasing test temperature. In contrast, the fracture modes of DIN 1.4926 and Ta remained transgranular up to the highest available doses of 7 and 11 dpa, respectively.
(4) The dominant microstructural feature is a high density of small 'black dot' defect clusters and dislocation loops in all materials. No bubbles could be observed in all investigated of as-irradiated materials.
(5) The suspicion that RIS at grain boundaries may have caused the intergranular failure of some 304L and IN 718 specimens is not supported by our data. However, AES meassurements [17] do show irradiation-induced changes of the elemental composition of IN 718 near (<10 nm) grain boundaries. An influence of RIS can therefore not be ruled out in this alloy.

These statements hold of course only for the available maximum dose of around 10 dpa, corresponding to a service time of about two months full power operation in ESS. There may be further reservation for the relevance of the above conclusions: Results obtained from spent targets have the advantage that they realistically reflect the actual service conditions of target components (changing power levels, i.e. varying temperatures and dose rates, short (accelerator trips) and long (service periods) down times). On the other hand, the complex and largely unknown irradiation history makes the allocation of the data to a particular set of parameters virtually impossible. Moreover, the varying conditions may mask effects which occur only in a narrow range of environmental parameters. An example for this possibility could be the drastic loss of uniform strain in austenitic steels irradiated and tested at 164 °C (see Fig. 4(b) and [14]), an effect which could not be reproduced in the present investigation.

The investigations of spent targets must therefore be supplemented by dedicated irradiation experiments with well defined and controlled conditions. This is achieved in the international collabration STIP (SINQ Target Irradiation Programme) started in 1998 [18] and in experiments utilizing the LANSCE Facility [14]. The first results of these experiments have been published elsewhere [14,19,20]. These efforts will extend and

consolidate the results from the investigation of spent targets and will lead to an extensive database which should allow (a) the selection of the optimum structural material(s) for the ESS targets and (b) a reliable prediction of the lifetimes (the service period) of critical target components.

Finally it should be mentioned that radiation damage is, of course, not the only criterion for materials selection. For example, in the window region of the mercury container the material must be able to withstand the high mechanical stresses, composed of (1) a pulsed stress caused by the pressure waves in the liquid mercury impinging on the container walls and (2) quasi-stationary thermal stresses due to the beam energy deposited in the wall materials itself. As illustrated in Fig. 14, the amplitudes of type (1) stresses are materials independent and decrease with increasing wall thickness d whereas type (2) stresses depend on the thermal conductivity and expansion of the materials and increase with d^2. Although the values in Fig. 14 are only rough estimates, they indicate that only martensitic steels and the Inconel alloy will have sufficient initial yield stresses to cope with the expected loads without large plastic deformation. Because of the high vulnerability to radiation-induced embrittlement of Ni-based high strength alloys, martensitic steels appear to be an acceptable compromise as candidate structural materials at present. An alternative are cold-worked austenitic steels which should exhibit better ductility and toughness at low temperatures. However, their use requires a component design which avoids weldments in region exposed to high irradiation loads. The situation may change if ongoing efforts to reduce the amplitude of the stress pulse are successful, e.g. by introducing small helium bubble into the mercury. The verification of such mitigation efforts has recently been intensified after discovering local erosion damage in steel surfaces in contact with a heavy liquid metal in which pressure waves have been induced [21]. It is suspected that this 'pitting' is caused by the collapse of cavities formed during the tensile phase of the pressure waves. A reduction of their amplitude would thus not only reduce the wall stresses but also solve the pitting problem. In this case, 'soft' materials such as solution annealed austenitic steels or even tantalum which retain relatively high ductility under irradiation could become promising candidate materials for structural target components in the ESS.

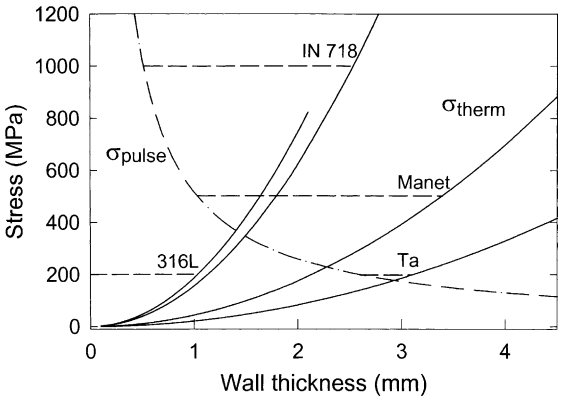

Fig. 14. Estimated stresses in the beam entrance region of the ESS target container. The solid and dot-dashed lines indicate thermal stresses and pulsed stresses, respectively. The initial yield strengths for different materials are also given, indicated by horizontal dashed lines.

Acknowledgements

The authors would like to thank Dr P. Jung for useful discussions. The authors are also grateful to the staff members of the hot cells of the Forschungszentrum Jülich for their support in specimen handling and preparation.

References

[1] ESS – A next generation neutron source for Europe, vol. III: The ESS Technical study, ESS Report 96-53-M (November 1996) ISBN 0902376500.
[2] Spallation Neutron Source at Oak Ridge, TN, USA. Available from <www.sns.gov/documentation/pubs.htm>.
[3] F. Carsughi, H. Derz, P. Ferguson, G. Pott, W.F. Sommer, H. Ullmaier, J. Nucl. Mater. 264 (1999) 78.
[4] J. Chen, Y. Dai, F. Carsughi, W.F. Sommer, G.S. Bauer, H. Ullmaier, J. Nucl. Mater. 275 (1999) 115.
[5] M.R. James, S.A. Maloy, F.D. Gac, W.F. Sommer, J. Chen, H. Ullmaier, J. Nucl. Mater. 296 (2001) 139.
[6] Y. Dai, G. Bauer, F. Carsughi, H. Ullmaier, S.A. Maloy, W.F. Sommer, J. Nucl. Mater. 265 (1999) 203.
[7] J. Chen, H. Ullmaier, T. Floßdorf, W. Kühnlein, R. Duwe, F. Carsughi, T. Broome, J. Nucl. Mater. 298 (2001) 248.
[8] S.L. Green, J. Nucl. Mater. 126 (1984) 30.
[9] M. Wechsler, M.H. Barnett, D.J. Dudziak, L.K. Mansur, L.A. Charlton, J.M. Narnes, J.O. Johnson, Proceedings of the Symposium on Materials for spallation Neutron Sources, Orlando, 10–12 February 1997.
[10] D. Filges, C. Mayr, R.D. Neef, H. Schaal, A. Tietz, J. Wimmer, ESS report no. 96-45-T (1996).
[11] F.A. Garner, B.M. Oliver, L.R. Greenwood, M.R. James, P.D. Ferguson, S.A. Maloy, W.F. Sommer, J. Nucl. Mater. 296 (2001) 66.
[12] B.H. Sencer, G.M. Bond, F.A. Garner, M.L. Hamilton, S.A. Maloy, W.F. Sommer, J. Nucl. Mater. 296 (2001) 145.
[13] J.D. Hunn, E.H. Lee, T.S. Byun, L.K. Mansur, J. Nucl. Mater. 296 (2001) 203.
[14] S.A. Maloy, M.R. James, G. Willcutt, W.F. Sommer, M. Sokolov, L.L. Snead, M.L. Hamilton, F. Garner, J. Nucl. Mater. 296 (2001) 119.

[15] J.D. Elen, P. Fenici, J. Nucl. Mater. 191–194 (1992) 766.
[16] Y. Dai, X. Jia, J. Chen, W.F. Sommer, M. Victoria, G.S. Bauer, J. Nucl. Mater. 296 (2001) 174.
[17] M. García-Mazarío, M. Hernández-Mayoral, A.M. Lancha, J. Nucl. Mater. 296 (2001) 192.
[18] Y. Dai, G.S. Bauer, J. Nucl. Mater. 296 (2001) 43.
[19] K. Farrell, T.S. Byun, J. Nucl. Mater. 296 (2001) 129.
[20] Y. Dai, Y. Foucher, M.R. James, B.M. Oliver, these Proceedings. doi:10.1016/S0022-3115(03)00099-0.
[21] K. Kikuchi, H. Kogawa, M. Futakawa, S. Ishikura, M. Kaminaga, R. Hino, these Proceedings. doi:10.1016/S0022-3115(03)00016-3.